Optimal Periodic Control of an Ideal Stirling Engine Model

Mitchel Craun[1]
Mechanical Engineering,
University of California, Santa Barbara,
Santa Barbara, CA 93106
e-mail: craun@umail.ucsb.edu

Bassam Bamieh
Mechanical Engineering,
University of California, Santa Barbara,
Santa Barbara, CA 93106

We consider an optimal control problem for a model of a Stirling engine that is actively controlled through its displacer piston motion. The framework of optimal periodic control (OPC) is used as the setting for this active control problem. We use the idealized isothermal Schmidt model for the system dynamics and formulate the control problem so as to maximize mechanical power output while trading off a penalty on control (displacer motion) effort. An iterative first-order algorithm is used to obtain the optimal periodic motion of the engine and control input. We show that optimal motion is typically nonsinusoidal with significant higher harmonic content, and that a significant increase in the power output of the engine is possible through the optimal scheduling of the displacer motion. These results indicate that OPC may provide a framework for a large class of energy conversion and harvesting problems in which active actuation is available.
[DOI: 10.1115/1.4029682]

1 Introduction

Stirling engines are heat air engines that can operate using any heat power source such as external combustion, waste heat, or solar thermal power. They are receiving renewed interest as a potentially competitive energy conversion technology in several domains including micro combined heat and power (such as the WhisperGen units made by WisperTech, Christchurch, New Zealand), and solar thermal energy conversion (such as those made by SunPower, Inc., Athens, OH and Infinia Corp., Ogden, UT).

There has been recent interest in more detailed modeling and optimization of Stirling engines and coolers [1]. Related recent work on control-oriented modeling of a Stirling engine was done in Refs. [2–5], while the concept of an Active Stirling Engine [6] has been recently proposed. This latter concept is similar to our current work, where the displacer piston motion is the control input. Rather than let displacer motion be determined by the mechanical engine design (whether in kinematically linked engines or the free-piston variety), this new Stirling engine concept is based on directly actuating the displacer piston. This provides a large amount of control authority over the engine dynamics. A natural question then is how to exploit this new control possibility to optimize the operation of the engine, and whether significant increases in efficiency and/or power output can be achieved. In contrast to Ref. [6], where the control objective is for the displacer to track a predetermined trajectory, we formulate a problem where the periodic piston motions and the thermodynamic cycle itself are optimally designed.

In this paper, we cast the active control problem of a Stirling engine as a problem in OPC. This is motivated by the observation that the ultimate motion of such devices is cyclical, but the optimal limit cycle is not known a priori, but is to be designed through the optimal control problem. We therefore do not have a traditional trajectory tracking problem, but rather a problem of optimal trajectory design with periodic boundary conditions, i.e., optimal limit cycle design. Since one of the main concerns with Stirling engines is their relatively low power density, we setup a problem where the mechanical power output is to be maximized while trading off the control effort.

This paper is organized as follows: Section 2 describes the dynamical model used, which is the so-called isothermal Schmidt model. This is the simplest possible model of a Stirling engine and is used as a proof-of-concept to illustrate the advantages of optimal cycle design. The methodology presented is, however, applicable to higher fidelity engine models as well. Section 3 sets up optimal cycle design as an OPC problem and presents the iterative numerical hill climbing algorithm we used. There are special issues introduced by the periodic boundary conditions which require careful treatment, and these are discussed in some detail. Finally, Section 4 presents a case study with numerical results, together with a comparison to a well-designed kinematically linked, beta-type Stirling engine. Significant output mechanical power improvement on the order of 40% was achieved for this example.

2 Dynamic Modeling

A Stirling engine is an air engine in which pressure oscillations drive a power piston that performs mechanical work on a load. These pressure oscillations are in turn driven by the mechanical motion of both power and displacer pistons. We present the simplest possible model for this engine, the so-called isothermal Schmidt model. The first model in Sec. 2.1 is that of an engine with an actuated displacer but without kinematic linkages between power and displacer pistons (Fig. 1(*c*)). We use this model for optimal cycle design. The second model in Sec. 2.2 has flywheel kinematic linkages, resulting in a so-called beta-type engine (Fig. 1(*b*)), which we use as a benchmark case for performance comparisons.

2.1 The Basic Isothermal Model. Figure 1(*a*) is a diagram of the basic compartments and pistons of a Stirling engine. The engine is composed of three sections, the hot and cold chambers and the regenerator. The hot chamber is in thermal contact with a heat source, and the cold chamber is in thermal contact with a heat sink. Gas can move between the two chambers through the regenerator channel. The power piston performs work on a load, while the displacer piston's primary task is to move the working gas between the hot and cold chambers through the regenerator. Mechanical motion induces thermodynamic changes as follows: as the displacer piston oscillates, air is shuttled between the hot and cold chambers through the regenerator channel. This shuttling creates oscillations in the average (over all sections) gas temperature, which in turn cause oscillations in engine pressure. The pressure oscillations drive the power piston, which is how the gas thermodynamics induce mechanical motion. In a beta-type engine such as the one shown in Fig. 1(*b*), the kinematic linkages provide a feedback path between the power piston motion and displacer

[1]Corresponding author.

Contributed by the Dynamic Systems Division of ASME for publication in the Journal of Dynamic Systems, Measurement, and Control. Manuscript received August 28, 2013; final manuscript received December 22, 2014; published online March 4, 2015. Assoc. Editor: John B. Ferris.

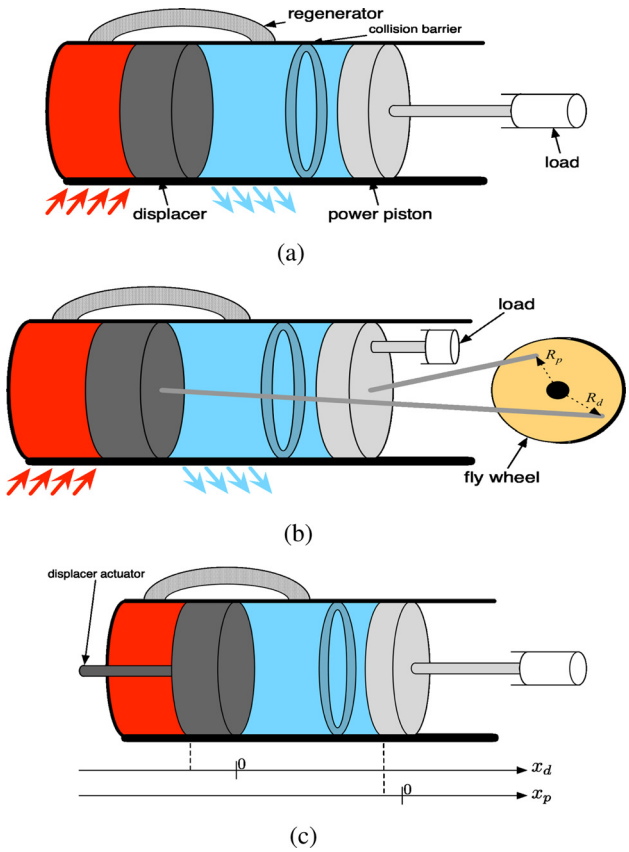

Fig. 1 Conceptual diagrams of Stirling engines where (*a*) shows the basic compartments and pistons, while (*b*) shows a beta-type engine where pistons are kinematically linked through a flywheel, and (*c*) shows the new concept of an engine with active control through direct actuation of the displacer piston. Linkages and actuators are shown conceptually and their actual geometry is not reflected in these diagrams.

piston, which shuttles the gas, and thus drives the gas thermodynamics. When the parameters are properly designed, this feedback creates self-sustaining oscillations in the engine.

In a Stirling engine, the regenerator is a channel filled with a porous metal matrix material. Its purpose is to act as a thermal capacitance, heating the cold air before it enters the hot section and cooling the hot air before it enters the cold section, thus significantly reducing loss of heat that is not converted to mechanical energy.

Mathematical models of such engines can be complex, but the isothermal Schmidt model is the simplest one and invokes the following assumptions:

(1) Mass is conserved, the gas obeys the ideal gas law, which is perfectly mixed in each section, and its kinetic energy is ignored.
(2) Pressure is uniform throughout the engine.
(3) The temperature profile in the regenerator is linear and interpolates between the temperatures of the adjacent hot and cold sections.
(4) The heat exchangers are perfect, so the temperatures of the hot and cold sections are constant in time (thus the term "isothermal") and equal to the temperatures of the heat source and sink, respectively. This is equivalent to the assumption that heat transfer between external reservoirs and the internal gas sections is instantaneous.

The first assumption is considered rather realistic, and subsequent ones are listed in increasing order of severity. Assumption 4 is perhaps the most drastic. It is popular since it simplifies mathematical modeling, at the expense of neglecting heat transfer dynamics which maybe significant in certain engines.

The above assumptions lead to a dynamical model derived below. The model derivations below are abbreviated since they are variations on a more detailed treatment available elsewhere [7]. If we denote power and displacer piston positions by x_p and x_d, respectively (see Fig. 1(*c*)), and power piston mass by m_p, then the mechanical portion of the dynamics is simply

$$\begin{aligned} m_p\ddot{x}_p &= F_P(x_p, x_d) - C_p\dot{x}_p \\ \dot{x}_d &= u(t) \end{aligned} \tag{1}$$

where C_p is the coefficient of a damper load through which power is extracted, and $F_p(x_p, x_d)$ is the pressure force on power piston to be discussed shortly. Displacers are typically very light, and therefore assumed massless. The control effort in this setting is related to the power needed to move the displacer back and forth. This is primarily related to pressure losses (viscous friction) within the regenerator loop. We will show these to be a function of displacer velocity, and we therefore choose that velocity (rather than displacer position) as the control input u. Of course, once optimal displacer velocity is determined, it is a simple matter to obtain optimal displacer displacement by integration.

2.1.1 Pressure Forces on Power Piston. In the isothermal model, temperatures in each section are assumed to be constant in time. Pressure is assumed to be uniform throughout all sections of the engine, but possibly time varying. Therefore, the volume oscillations of the hot and cold chambers, which are caused by the motion of the displacer and power piston, create oscillations in average gas temperature, which in turn creates pressure oscillations. This shows that the pressure force on the power piston is a function $F_p(x_p, x_d)$ of only those two dynamic variables.

The total gas mass in the engine is $m_t = m_c + m_r + m_h$, where m_c, m_r, and m_h are the masses of the gas in the cold, regenerator, and hot sections, respectively. In each section, the ideal gas law expresses this mass as $m = PV/RT$, where R is the gas constant, V and T are volume and temperature of the respective section (pressure P is assumed equal for all sections). We note that since the temperature in the regenerator is not spatially uniform, the relation $m_r = PV_r/RT_r$ needs to be interpreted in the sense of an "effective regenerator temperature" T_r, an issue which will be addressed shortly. Therefore, the ideal gas law implies that the total mass is

$$m_t = \frac{P}{R}\left(\frac{V_c}{T_c} + \frac{V_r}{T_r} + \frac{V_h}{T_h}\right) \tag{2}$$

Note that V_r is constant, while the volumes of the hot and cold chambers are functions of piston displacements

$$\begin{aligned} V_h &= V_{ho} + A_d x_d \\ V_c &= V_{co} - A_d x_d + A_p x_p \end{aligned} \tag{3}$$

where A_d and A_p are the cross-sectional areas of the displacer and power piston, respectively, and V_{ho} and V_{co} are the nominal volumes (at $x_p = x_d = 0$) of the hot and cold chambers, respectively. Equations (2) and (3) can now be solved to obtain pressure as a function of piston displacements x_p and x_d. It remains to calculate the effective regenerator temperature T_r.

The regenerator is assumed to be a linear, one-dimensional element with a temperature distribution $T(l) = T_h - (T_h - T_c/L)l$ which linearly interpolates the boundary temperatures T_h and T_c over the interval $l \in [0, L]$. Using the ideal gas law in each infinitesimal cross section gives the total regenerator mass as

$$m_r = \int_0^L \frac{P(A_r dl)}{RT(l)} = \int_0^L \frac{P}{R\left(T_h - \dfrac{T_h - T_c}{L}l\right)} A_r dl$$

where A_r is the cross-sectional area through which fluid can flow in the regenerator. This integral yields

$$m_r = \frac{PV_r}{R(T_h - T_c)} ln\left(\frac{T_h}{T_c}\right) \tag{4}$$

where V_r is the volume of the regenerator. We now observe that Eq. (4) is an ideal gas law for the regenerator if its temperature is taken as

$$T_r := \frac{T_h - T_c}{ln\left(\frac{T_h}{T_c}\right)} \tag{5}$$

Solving Eq. (2) for pressure and substituting for the variables V_h, V_c, and T_r from Eqs. (3) and (5) gives

$$P = \frac{m_t R}{\left(\frac{V_c}{T_c} + \frac{V_r}{T_r} + \frac{V_h}{T_h}\right)}$$

$$P = \frac{m_t R}{\left(\frac{V_{co}}{T_c} + \frac{V_{ho}}{T_h} + \frac{V_r ln\left(\frac{T_h}{T_c}\right)}{T_h - T_c} - \frac{A_d}{T_c}x_d + \frac{A_p}{T_c}x_p + \frac{A_d}{T_h}x_d\right)} \tag{6}$$

For notational clarity, the following constants are defined:

$$a_p := \frac{A_p}{T_c V_{mt}}, \quad a_d := \frac{A_d}{V_{mt}}\left[\frac{1}{T_c} - \frac{1}{T_h}\right]$$

$$V_{mt} := \frac{V_{ho}}{T_h} + \frac{V_r ln\left(\frac{T_h}{T_c}\right)}{T_h - T_c} + \frac{V_{co}}{T_c}$$

and the expression (6) can be more clearly rewritten as a function of piston displacements

$$P = \frac{m_t R}{V_{mt}}\left(\frac{1}{1 + a_p x_p - a_d x_d}\right) \tag{7}$$

The above expression for the pressure finally gives the pressure force term $F_p(x_p, x_d)$ in Eq. (1), and the engine dynamics can now be rewritten as

$$m_p \ddot{x}_p = A_p P_m \left[\frac{1}{1 + a_p x_p - a_d x_d} - 1\right] - C_p \dot{x}_p$$

$$\dot{x}_d = u(t) \tag{8}$$

where $P_m := m_t R / V_{mt}$ is the nominal pressure (at $x_p = x_d = 0$), which is also assumed to be equal to the pressure on the external side of the power piston.[1]

2.1.2 Pressure Losses in Regenerator and Control Power. Although in the derivation, pressure was assumed uniform throughout the engine, there is in reality a small pressure drop due to viscous friction when fluid flows across the regenerator matrix material. In an actively controlled Stirling engine (Fig. 1(*c*)), the actuator primarily works against that small pressure drop, which we need to characterize in order to quantify control effort. We point out that this pressure drop is typically much smaller than the pressure oscillations in the engine, which is the reason it can be neglected when calculating the force on the power piston in the previous section. This fact is recognized in traditional Stirling engines. It is also true in our controlled engine with optimally designed cycle as a consequence of the optimization objective (18). Maximization of this objective has the consequence of insuring that viscous losses (which are related to control power) are kept at a minimum compared with pressure oscillations (which determine the output power of the engine).

A standard model [7] for viscous pressure loses assumes them to be in the same direction as the average flow velocity v_r, but proportional in magnitude to its square

$$\Delta P = \frac{\rho_r f L}{r_h}(v_r)^2_{\pm} \tag{9}$$

where we have used the following notation for the "signed square" function $(\alpha)^2_{\pm} := \alpha|\alpha|$. The constants in the above expression are the fluid density ρ_r, f is the Fanning friction factor, L the length of the regenerator, and r_h is the hydraulic radius.

By conservation of mass, the average flow velocity v_r can be related to the cold and hot sections' mass flow rates by

$$\rho_r v_r A_r = \frac{1}{2}(\dot{m}_c - \dot{m}_h) = \frac{1}{2}\frac{d}{dt}(\rho_c V_c - \rho_h V_h) \tag{10}$$

where ρ_c and ρ_h are the fluid densities in the cold and hot sections, respectively. Using the ideal gas law with the assumption that pressure is uniform throughout, the densities can be expressed as

$$\rho_r = \frac{P}{RT_r}, \quad \rho_h = \frac{P}{RT_h}, \quad \rho_c = \frac{P}{RT_c} \tag{11}$$

The relative amplitudes of density oscillations are typically very small and therefore taken as constant. This simplifies the time derivative in Eq. (10) and yields the following expression for regenerator flow velocity as a function of the pistons' velocities:

$$v_r = \frac{T_r}{2A_r}\left(\frac{A_p}{T_c}\dot{x}_p - \frac{A_d(T_c + T_h)}{T_c T_h}\dot{x}_d\right) \tag{12}$$

This last expression for v_r and the expression (9) for the pressure loss now give an expression for the control power required in terms of the state variables and input. If the displacer piston is assumed to be nearly massless, then the force F_d needed to drive the displacer is equal and opposite to the force due to pressure difference across the displacer, which is just the pressure loss in the regenerator. The instantaneous control power is therefore the product of that force with displacer velocity yielding

$$\text{Instantaneous control power} = F_d \dot{x}_d = (-A_d \Delta P)\dot{x}_d$$

$$= \frac{A_d \rho_r f L T_r^2}{4 r_h A_r^2}\left(\frac{A_d(T_c + T_h)}{T_c T_h}\dot{x}_d - \frac{A_p}{T_c}\dot{x}_p\right)^2_{\pm}\dot{x}_d \tag{13}$$

2.2 Model of a Beta-Type Engine. This traditional type of Stirling engine has kinematic linkages and no active control. We use it as a benchmark design for performance comparison with our engine with optimally designed cycle. A typical beta Stirling engine design is shown in Fig. 1(*b*). Any parameters in common between the beta engine and the actively controlled one (Fig. 1(*c*)) were set equal. The main difference between the two is that kinematic linkages enforce constraints between the power and displacer piston motions. The dynamics for the beta engine can be written down using the model (8) and the geometrical relations from Fig. 1(*b*) as follows:

$$m_p \ddot{x}_p = A_p P_m \left[\frac{1}{1 + a_p x_p - a_d x_d} - 1\right] - C_p \dot{x}_p - F_p \tag{14}$$

$$I\ddot{\theta} = F_p R_p \sin(\theta - \phi) - A_d R_d \Delta P \sin(\theta) \tag{15}$$

[1]In other words, the origins of the x_p and x_d axes are chosen such that at $x_p = x_d = 0$, internal engine pressure is equal to the external atmospheric pressure. This makes the zero state an equilibrium of the dynamics.

$$x_d = -R_d \cos(\theta) \tag{16}$$

$$x_p = -R_p \cos(\theta - \phi) \tag{17}$$

where I and θ are the moment of inertia and angular position of the flywheel, respectively, F_p is the reaction force between the power piston and the flywheel, ϕ is the phase difference between the two pistons, R_p and R_d are the radial attachment locations of the pistons on the flywheel, and ΔP is the pressure difference across the displacer caused by forcing the working fluid to flow through the regenerator (Eq. (9)). These equations were derived assuming that the displacer and the arms connecting the pistons to the flywheel are massless. The latter are assumed to be sufficiently long so that the forces they exert on the flywheel and pistons are essentially horizontal.

3 Optimal Cycle Design

The goal is to find the cyclical displacer motion which will maximize the average *net power* produced by the Stirling engine over one period. We formulate this problem as an OPC problem, which is a standard optimal control problem, but with periodic boundary conditions. We then outline a first-order numerical method referred to as "hill climbing" to maximize the objective. The issue of enforcing periodic boundary conditions on both the state and co-state equations requires some special care which is expounded on in Sec. 3.3.

OPC has been an area of active research in the past, and it would be difficult to give a complete background here. Some of the more notable work [8–12] was partially motivated by energy efficiency problems starting in the 1970s. That work was dominated by the question of when cycling is more efficient than steady operation. However, here we have a slightly different setting in that the engines we deal with naturally (i.e., without control) would cycle. The availability of a control input then gives the additional design freedom of finding non-natural limit cycles that are energetically more favorable. The basic theoretical framework of OPC is, however, common to our present work and the earlier literature.

3.1 Optimal Control Problem Formulation. Power is extracted from the engine via a damper attached to the power piston, and some power is used up by the displacer actuator to work against viscous pressure losses across the regenerator. The average net power over one cycle is the difference between the two and is given by

$$J = \frac{1}{T}\int_0^T \phi(x,u)dt = \frac{1}{T}\int_0^T \left(C_p \dot{x}_p^2 - F_d u\right)dt \tag{18}$$

The dynamics are given by Eq. (8) and the control power $F_d u$ is

$$F_d u = \alpha\left(\alpha_d u - \alpha_p \dot{x}_p\right)_{\pm}^2 u \tag{19}$$

where the constants α, α_d, and α_p are given by Eq. (13). The period T is fixed in this formulation, and a search of a set of periods is done as an outer loop in the algorithm. All states and the control are required to satisfy *periodic boundary conditions*

$$\begin{aligned} &x_p(0) = x_p(T), \quad \dot{x}_p(0) = \dot{x}_p(T), \quad x_d(0) = x_d(T), \\ &u(0) = u(T) \end{aligned} \tag{20}$$

A final constraint we require is that of no collision between the pistons and the collision barrier or the engine walls. These can be expressed using the inequality constraints

$$\begin{aligned} &\underline{L}_d \le x_d(t) \le \bar{L}_d \\ &\underline{L}_p \le x_p(t) \end{aligned} \tag{21}$$

where $\underline{L}_d, \underline{L}_p$, and $\bar{L}_d$ are the lower and upper limits on the displacer and power pistons' positions, respectively. Hard limit constraints such as these are typically difficult to enforce in numerical optimal control problems, so a "soft constraints" approach is used by augmenting the objective with suitably designed penalty functions P_d and P_p that grow unboundedly as the states approach the constraints

$$J = \frac{1}{T}\int_0^T \left(C_p \dot{x}_p^2 - F_d u - P_d(x_d) - P_p(x_p)\right)dt \tag{22}$$

In summary, our optimal control problem has the dynamics

$$\begin{aligned} \dot{x}_1 &= x_2 \\ \dot{x}_2 &= \frac{A_p P_m}{m_p}\left[\frac{1}{1 + a_p x_1 - a_d x_3} - 1\right] - \frac{C_p}{m_p} x_2 \\ \dot{x}_3 &= u \end{aligned} \tag{23}$$

where $x_1 := x_p$, $x_2 := \dot{x}_p$, and $x_3 := x_d$. The boundary conditions (20) are T-periodic. The objective is to maximize the performance

$$J = \frac{1}{T}\int_0^T \left(C_p x_2^2 - \alpha\left(\alpha_d u - \alpha_p x_2\right)_{\pm}^2 u - P_d(x_3) - P_p(x_1)\right)dt \tag{24}$$

3.1.1 First-Order Variations. In deriving first-order necessary conditions for optimality as well as first-order numerical algorithms, it is useful to calculate variations using a costate as a Lagrange multiplier. These calculations are standard in any optimal control textbook [13–15], so we only recap what we need here to highlight the role of periodic boundary conditions. Consider an optimal control problem with the dynamical constraint

$$\dot{x} = f(x,u), \qquad x(0) = x(T) \tag{25}$$

and the performance objective $J = (1/T)\int_0^T \phi(x,u)dt$. A Lagrangian objective $\mathcal{J}$ is defined using a Lagrange multiplier function $\lambda(t)$, $t \in [0, T]$ termed the costate by

$$\mathcal{J} := \frac{1}{T}\int_0^T \left(\phi(x,u) - \lambda^T(\dot{x} - f(x,u))\right)dt \tag{26}$$

The standard calculus of variations argument including an integration by parts yields the following expression for the variations in $\mathcal{J}$:

$$\begin{aligned} \delta\mathcal{J} = \frac{1}{T}\Bigg(&\int_0^T \left[\frac{\partial\phi}{\partial x} + \dot{\lambda}^T + \lambda^T \frac{\partial f}{\partial x}\right]\delta x\, dt - [\lambda^T(T) - \lambda^T(0)]\delta x(0) \\ &+ \int_0^T \left[\frac{\partial\phi}{\partial u} + \lambda^T \frac{\partial f}{\partial u}\right]\delta u\, dt\Bigg) \end{aligned} \tag{27}$$

where the state equation $\dot{x} = f(x,u)$ and its periodic boundary conditions $x(0) = x(T) \Rightarrow \delta x(0) = \delta x(T)$ have been used. If in addition, the costate is forced to satisfy the following adjoint equation with periodic boundary conditions:

$$\dot{\lambda} = -\left(\frac{\partial f}{\partial x}\right)^T \lambda - \left(\frac{\partial \phi}{\partial x}\right)^T, \qquad \lambda(0) = \lambda(T) \tag{28}$$

then variations in $\mathcal{J}$ can finally be expressed as

$$\delta\mathcal{J} = \frac{1}{T}\int_0^T \left[\frac{\partial\phi}{\partial u}(x,u) + \lambda^T \frac{\partial f}{\partial u}(x,u)\right]\delta u\, dt \tag{29}$$

where u, x, and λ satisfy Eqs. (25) and (28). When deriving first-order necessary conditions for optimality, the term in square

brackets in Eq. (29) is set to zero. Alternatively, this expression for $\delta\mathcal{J}$ is used to propose updates to control inputs in an iterative numerical algorithm, which is presented in the next section.

3.2 Hill Climbing. Expression (29) can be used to build an iterative algorithm for maximizing the objective (thus the term "hill climbing"). The initialization step consists of applying some periodic input u_0 to the system and obtaining the corresponding periodic state trajectory x_0. For each subsequent step, let (u_n, x_n) be the functions obtained at the nth step of the algorithm, then the next iteration is chosen according to

$$\dot{\lambda}_n = -\left(\frac{\partial f}{\partial x}(x_n, u_n)\right)^T \lambda_n - \left(\frac{\partial \phi}{\partial x}(x_n, u_n)\right)^T$$
$$\lambda_n(T) = \lambda_n(0) \tag{30}$$

$$u_{n+1} = u_n + \varepsilon\left(\frac{\partial \phi}{\partial u}(x_n, u_n) + \lambda_n^T \frac{\partial f}{\partial u}(x_n, u_n)\right) \tag{31}$$

$$\dot{x}_{n+1} = f(x_{n+1}, u_{n+1}), \qquad x_{n+1}(T) = x_{n+1}(0) \tag{32}$$

Several remarks can be made about this algorithm

- Since (u_n, x_n, λ_n) simultaneously satisfy the sate and costate equations, the expression (29) for the variation guarantees that if $(\delta u)_n := u_{n+1} - u_n$ is chosen according to Eq. (31), then

$$\delta\mathcal{J} = \frac{1}{T}\int_0^T \left[\frac{\partial \phi}{\partial u}(x, u) + \lambda^T \frac{\partial f}{\partial u}(x, u)\right]^2 dt \geq 0$$

  and thus there exists a sufficiently small step size ε such that the value of the objective at step $n+1$ is improved over that at step n.
- Both Eqs. (32) and (30) require finding T-periodic solutions to the corresponding differential equations. These issues are carefully addressed in Sec. 3.3.

The method just described is a standard one in numerical optimal control and was first used for *periodic* optimal control problems by Horn and Lin [16]. Similar methods have also been used by Kowler and Kadlec [17] and van Noorden et al. [18]. There are two main distinctions between their algorithms and ours. The first is that the existence of *periodic* solutions to the costate equation (28) was implicitly assumed and not addressed in Refs. [16–18]. These equations do not always admit periodic solutions, and we analyze conditions that guarantee existence in the sequel. The second distinction is in how the periodic state and costate trajectories are determined. A Newton–Raphson iteration is used in Refs. [16] and [17] to find the periodic state trajectories, and then the costate trajectories are found by a decomposition into homogeneous and particular solutions. A more sophisticated Newton–Picard iterative algorithm is used in Ref. [18] to solve for both the state and costate trajectories. In the present work, the state trajectories were found by simply simulating the state equations for sufficiently long times to reach periodic steady-state conditions. For problems with slow dynamics, it is preferable to use an iterative method to find the periodic state trajectories associated with a given input. However, the dynamics associated with our problem converged relatively quickly, so the added complexity associated with an iterative routine was not deemed necessary. To find the periodic costate trajectories, we developed an algorithm described in Sec. 3.3, which uses the variation of constants formula to find the periodic boundary conditions directly.

3.3 Enforcing Periodicity. We begin with enforcing the periodicity of the state equation (32) as it is the simpler case. Since the input enters the dynamics through an integrator (the equation for $\dot{x}_3$ in Eq. (23)), a necessary condition for x_3 to be periodic is for u to have zero average in time. Therefore, the zero-average constraint on controls needs to be added to our OPC problem. It is not difficult to show[2] that this amounts to simply removing any DC component of u_{n+1} in Eq. (31) at every step of the iteration. While this is a necessary but not sufficient condition for the periodicity of the state trajectory, it was found through extensive numerical experiments that this condition alone resulted in a T-periodic steady-state trajectory (after simulation over several cycles) of Eq. (32) when the input is T-periodic and has zero mean. This is likely due to the physical nature of this particular model.

As for the costate equation (28), note that it is a linear, periodically time-varying system (for λ) where the function $(\partial\phi/\partial x)^T$ is an input. It is thus of the form

$$\dot{\lambda}(t) = A(t)\lambda(t) + B(t), \qquad \lambda(0) = \lambda(T) \tag{33}$$

where both $A(.)$ and $B(.)$ are periodic functions with period T. The periodic boundary condition $\lambda(0) = \lambda(T)$ amounts to requiring this equation to have a T-periodic solution. However, it is not always true that a linear T-periodically time-varying system with a T-periodic input must have a T-periodic trajectory, more complex behavior can occur [19]. Here, we give conditions for the required periodic solution to exist, and then show how the additional flexibility available through selecting penalty functions can be used to insure this condition is satisfied.

First, we show how all initial conditions leading to T-periodic solutions can be characterized. Using the variations-of-constants formula on (33) gives

$$\lambda(T) = \Phi(T, 0)\lambda(0) + \int_0^T \Phi(T, t)B(t)dt \tag{34}$$

where Φ is the state transition matrix of the system. Now the existence of an initial condition leading to a periodic solution $\bar{\lambda} = \lambda(0) = \lambda(T)$ is equivalent to the existence of a vector $\bar{\lambda}$ that solves the following matrix–vector equation:

$$(I - \Phi(T, 0))\bar{\lambda} = \int_0^T \Phi(T, t)B(t)dt \tag{35}$$

We note that if such initial conditions exist, their calculation is a linear algebra problem. The vector $\int_0^T \Phi(T, t)B(t)dt$ is calculated from a simulation of a linear system with zero initial conditions, while the matrix $\Phi(T, 0)$ can be calculated in the standard manner from a number of linear initial value problems. After these calculations, the linear system of equations (35) can be solved for $\bar{\lambda}$.

It now remains to provide conditions as to when the system (35) has solutions $\bar{\lambda}$, or equivalently as to when the linear, T-periodic system (33) has T-periodic solutions. This question has previously been addressed in the literature [19]. We rephrase the main result here in a form that is directly applicable to the present problem.

THEOREM 1. *The following three statements are equivalent*:

- *The linear T-periodic system*

$$\dot{\lambda}(t) = A(t)\lambda(t) + B(t) \tag{36}$$

  has a T-periodic solution, i.e., such that $\lambda(0) = \lambda(T)$.
- *The following matrix–vector equation has a solution $\bar{\lambda}$:*

$$(I - \Phi(T, 0))\bar{\lambda} = \int_0^T \Phi(T, t)B(t)dt \tag{37}$$

[2]This follows from the observation that $u_{n+1} - n_n$ needs to be in the direction δu that maximizes (29) subject to the constraint of zero average. This direction is simply the projection of the square bracketed term onto the subspace of zero-average signals, i.e., removing the DC term.

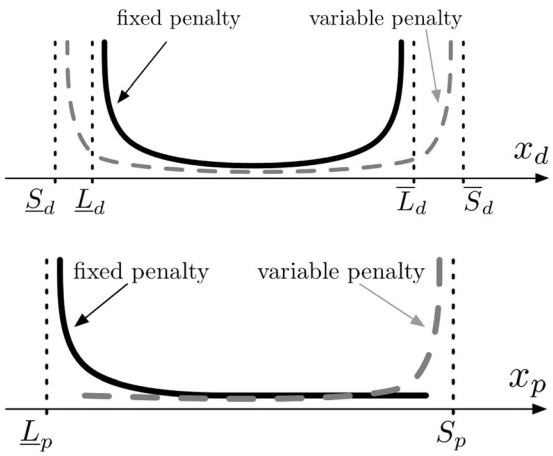

Fig. 2 A schematic of the fixed and variable penalties on the displacer (top) and power (bottom) pistons' positions. The variable penalties' shifts S_p, $\underline{S}_d$, and $\bar{S}_d$ are parameters determined at each iteration step of the algorithm to enforce condition (40).

where Φ is the state transition matrix of A.

- *For any T-periodic solution z of the homogenous adjoint system $\dot{z}(t) = -A^*(t)z(t)$, the following orthogonality condition holds:*

$$\int_0^T z^T(t)B(t)dt = 0 \tag{38}$$

Furthermore, each T-periodic solution of Eq. (36) is such that $\lambda(0) = \bar{\lambda}$, where $\bar{\lambda}$ is a solution to Eq. (37), and vice versa, i.e., there is a one-to-one correspondence between T-periodic solutions of Eq. (36) and vector solutions of Eq. (37).

This theorem is a reformulation of a result in Ref. [19], Sec. 2.10, Lemma I. For completeness, we provide a brief, self-contained proof in the Appendix. Condition (38) can be used to check whether a given system has T-periodic solutions, then solutions of the matrix–vector equation (37) are used to find the corresponding initial conditions, and thus the T-periodic solutions.

To see the consequences of condition (38) to the present problem, Eq. (30) is written out explicitly after reference to the dynamics (23) and performance objective (24)

$$\begin{bmatrix} \dot{\lambda}_1 \\ \dot{\lambda}_2 \\ \dot{\lambda}_3 \end{bmatrix} = \begin{bmatrix} 0 & \dfrac{a_p(A_pP_m/m_p)}{(1+a_px_1-a_dx_3)^2} & 0 \\ -1 & \dfrac{C_p}{m_p} & 0 \\ 0 & \dfrac{-a_d(A_pP_m/m_p)}{(1+a_px_1-a_dx_3)^2} & 0 \end{bmatrix} \begin{bmatrix} \lambda_1 \\ \lambda_2 \\ \lambda_3 \end{bmatrix} - \begin{bmatrix} P_p'(x_1) \\ \dfrac{\partial\phi}{\partial x_2} \\ P_d'(x_3) \end{bmatrix} \tag{39}$$

where P' stands for the derivative of the corresponding single-variable function P, and the exact form of $\partial\phi/\partial x_2$ is irrelevant in the sequel. To apply Theorem 1, we note that $A := -(\partial f/\partial x)^T$ above has the following left null vector:

$$v_n = [\,a_d \quad 0 \quad a_p\,]$$

for any state trajectory. This implies that $z_n := v_n^T$ is always a right null vector for the adjoint system $\dot{z} = -A^T(t)z$, and thus gives constant (and therefore T-periodic) solutions. Condition (38) applied to this solution $z^T(t) = [\,a_d \quad 0 \quad a_p\,]$ gives the requirement

$$\int_0^T \Big(a_dP_p'(x_1(t)) + a_pP_d'(x_3(t))\Big)dt = 0 \tag{40}$$

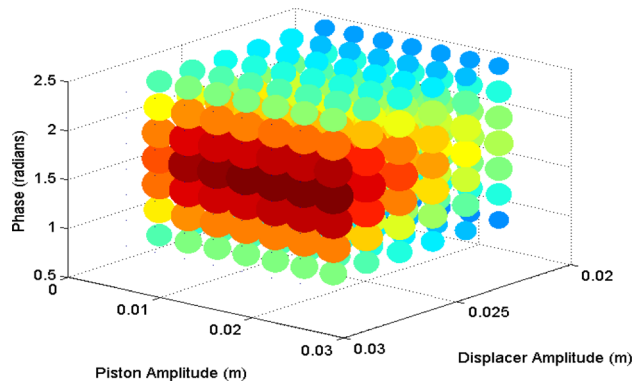

Fig. 3 A plot showing the effect of three parameters of a beta engine on power output. The parameters are the phase difference, displacer, and piston amplitude. Small blue spheres represent small objective values while large dark red spheres represent large objective values. The small dots represent points that either does not produce limit cycles or results in collisions. The optimal phase is around 90 deg, power piston amplitude has relatively little effect on performance, while larger displacer amplitudes produce more power.

Extensive numerical investigations were carried out, and no other periodic solutions of the homogenous system adjoint to Eq. (39) were found. We thus proceed with the assumption that condition (40) is the only one that needs to be checked.

In our routines, the constraint (40) is enforced on each term in the integral separately. Consider the displacer position penalty first. A sketch of a typical P_d is shown in Fig. 2, where it is termed the "fixed penalty." This penalty has even symmetry about the midpoint of $[\underline{L}_d, \bar{L}_d]$, and therefore P_d' has corresponding odd symmetry.[3] If the trajectory of x_d is symmetric in time about the midpoint, then clearly the integral of $P_d'(x_d(t))$ over one periodic will be zero. However, as is typical in the initial steps of the algorithm, x_d may not have that temporal symmetry. We therefore augment P_d with an additional function (termed "variable penalty" in Fig. 2), which has variable parameters $\underline{S}_d$ and $\bar{S}_d$. These parameters essentially bias the even symmetry of the augmented P_d (and consequently the odd symmetry of P_d'). Therefore even when the trajectory x_d does not have temporal symmetry about the midpoint, parameters $\underline{S}_d$ and $\bar{S}_d$ can be found such that the integral of the augmented $P_d'(x_d(t))$ is zero over one period. This augmented penalty function retains the barrier penalty features at $\underline{L}_d$ and $\bar{L}_d$ of the original one and has the additional property of satisfying the integral constraint. A similar technique is used for the power piston penalty function as illustrated in the bottom part of Fig. 2. Those details are omitted for brevity. Finally, we note that at each step of the iteration, the parameters $\underline{S}_d, \bar{S}_d$, and S_p required to enforce Eq. (40) are found using a zero finding routine such as "fzero" in MATLAB.

3.3.1 The Case of Multiple Solutions. Much of the above discussion was aimed at insuring the existence of a solution to the costate equation (30). It is possible that this equation may have multiple solutions as well (though this case was not encountered in the present work). In such cases, the multiplicity of solutions can help the objective improvements at each step. The set of solutions of Eq. (30) is a linear affine space completely characterized by solutions of the vector equation (37). The "steepest direction" δu to take in Eq. (29) is the one that corresponds to the λ amongst all solutions of Eq. (30) that maximizes the L^2 norm of the square bracketed term in Eq. (29). This is a convex, finite-dimensional, quadratic optimization problem where the number of variables is

[3]In our particular implementation, all penalty functions (fixed and variable) are sums of reflections and shifts of a one-sided penalty function used as a basic building block.

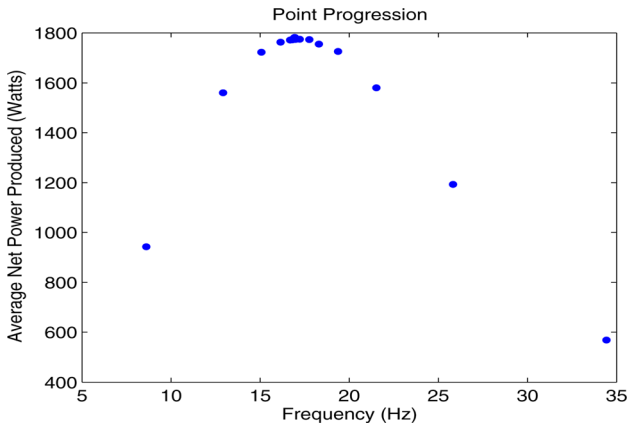

Fig. 4 The maximum average net power produced by the actuated Stirling engine as a function of displacer frequency. The peak in power production occurs at around 17 Hz.

precisely the number of linearly independent solutions of Eq. (30).

3.4 Summary of the Algorithm. The hill climbing method with periodicity enforcement is now summarized. The following procedure is done for each fixed periodic T. The procedure is initialized by choosing a suitable starting control input u_0 (e.g., a sinusoid), simulating the open-loop dynamics over several cycles until a steady-state periodic solution is reached. This provides the initializing trajectories (u_0, x_0) for Eq. (30).

Steps 1 and 2 below are repeated iteratively within two loops. The innermost loop repeats the steps until no significant improvement in the performance objective is observed. The outermost loop then "tightens" the penalty functions, i.e., increases the steepness of the penalty functions (c.f., Fig. 2) so that these soft constraints effectively enforce the hard limits (21).

(1) Given (u_n, x_n), solve Eq. (30) for λ_n. This requires the following steps.
(2) Using a zero finding routine, determine parameters $\underline{S}_d, \bar{S}_d$, and S_p to ensure condition (40) for the augmented penalty functions is satisfied. This guarantees the existence of a periodic solution to the costate equations.
(3) Solve the costate equation (30). This is done by solving Eq. (35) for the initial condition $\bar{\lambda}$ that will yield a periodic solution. The state transition matrix and input in Eq. (35) refer to the system (39).
(4) Calculate u_{n+1} using Eq. (31), and then x_{n+1} is found by simulating Eq. (32) until a periodic steady-state is reached. The step size ε is chosen small enough to insure improvement in the objective function and to avoid collisions.

4 Case Studies

The optimization framework discussed in the pervious section was applied to a Stirling engine model where the displacer piston motion is the control input, and a performance comparison with a standard kinematically linked Stirling engine was performed. We chose a so-called beta-type engine as a benchmark case for comparison. Such an engine has several design parameters that need to be chosen for satisfactory performance. An important consideration is that a fair comparison should be done to a "well-designed" benchmark case. Since there are currently no universally agreed-upon standardized Stirling engine designs, we have chosen to parametrically optimize a beta-type engine to serve as our benchmark reference. Other basic parameters of the engines that are not to be optimized (such as reservoir temperatures, cylinder areas, and nominal pressure) are taken from Ref. [7].

4.1 Benchmark: Parametrically Optimized Beta Engine. The benchmark engine used is the beta model described in Sec. 2.2. This engine has several design parameters including the flywheel and its kinematic linkages ϕ, R_p, R_d, and I. A standard nonlinear programming method of optimization was applied to obtain the parameter values producing the maximum average power over one engine cycle. The objective function used was Eq. (18), with the term accounting for power loss from displacer actuation removed. It was found that changing I served mainly to change the time needed for the engine to reach steady-state, but had little effect on the resulting power produced at steady-state. Therefore, I was chosen as constant and not a parameter in the optimization routine. The constraints were that the radii must be positive, while being small enough to prevent collisions with the

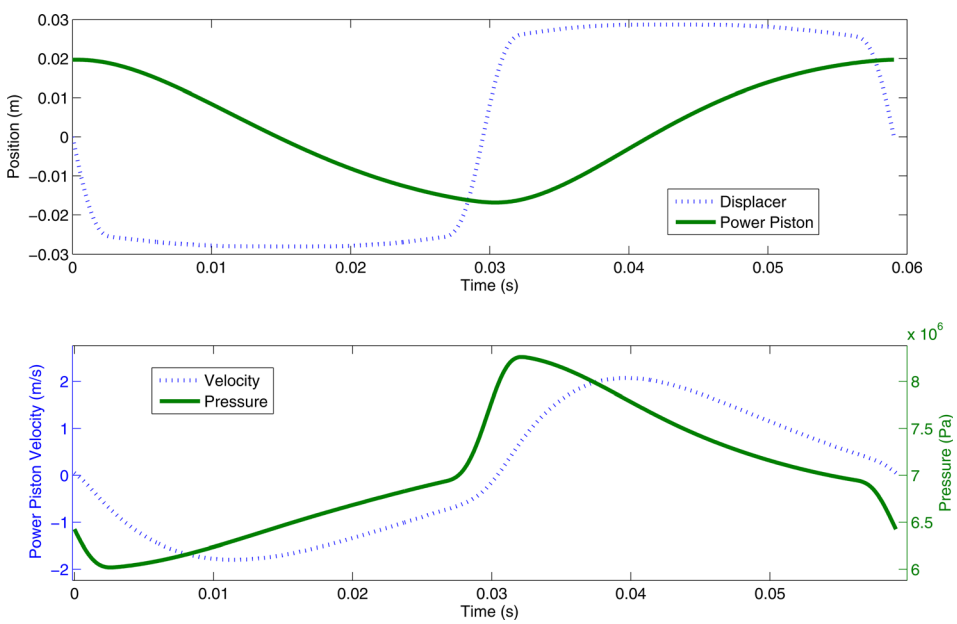

Fig. 5 The optimal motions and the pressure and velocity curves are displayed here for the actuated displacer model. The optimal displacer motion resembles that of a square wave. This maximizes the time spend at both pressure extremes.

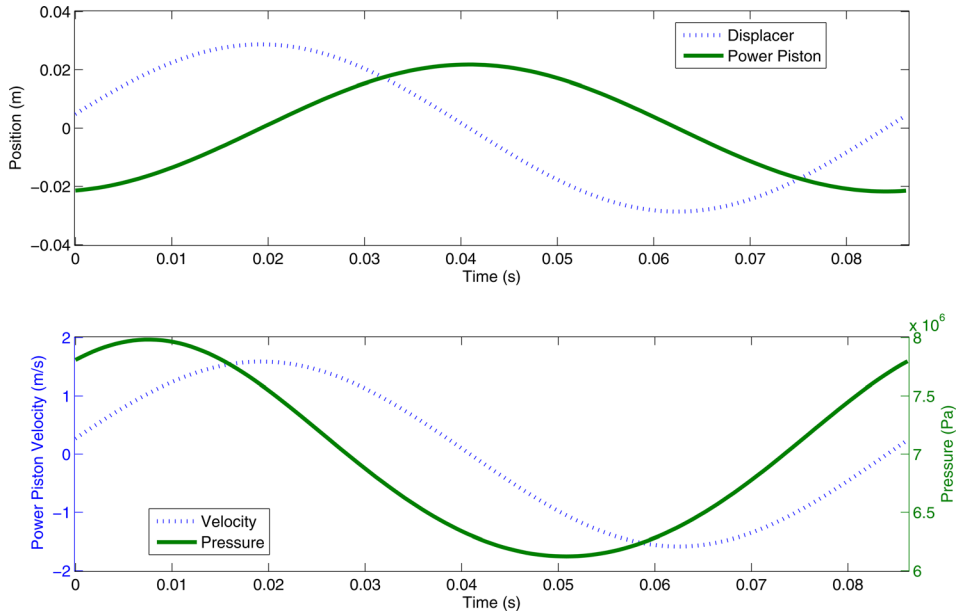

Fig. 6 The optimal motions and the pressure and velocity curves are displayed here for the beta Stirling model. The optimal piston motions resemble that of a sine wave. This is a result of the rotational inertia causing the flywheel to spin at near constant speed.

engine wall and the collision barrier. The fmincon routine in MATLAB was used to find the optimal radii and the phase difference. The function called by fmincon simulated the beta engine given the radii and phase differences. Once the engine reached steady-state, the function returned the rate of power extraction to fmincon.

Figure 3 shows the engine's net mechanical power output as a function of the three design variables. This figure illustrates that power output is relatively insensitive to power piston amplitude, while optimal phase is close to 90 deg, and that larger displacer piston motions (limited by constraints that avoid collisions) produce higher power.

4.2 Performance With Optimal Cycle Design. The periodic optimal control algorithm was used to optimize the operating cycle of a displacer-actuated version of the parametrically optimized beta engine. For a range of operating frequencies, the algorithm was executed and Fig. 4 shows the resulting maximum average net power as a function of frequency. The maximum average net power produced was just under 1800 W at approximately 17 Hz.

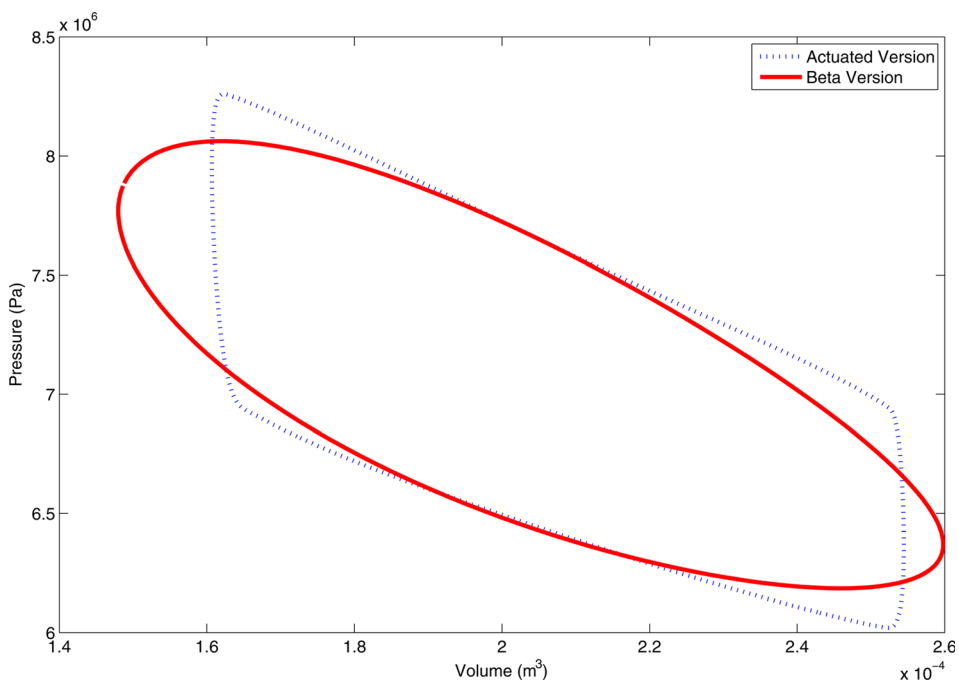

Fig. 7 A PV diagram showing the optimally actuated cycle and the optimal beta cycle. The curves proceed clockwise and the area enclosed by the either curve is the mechanical energy output (per cycle) of the engine.

At the frequency corresponding to maximum net power, optimal displacer and power piston trajectories are shown in Fig. 5. Note that displacer motion is closer to a square wave than a pure sinusoid; this maximizes the time spent at the two pressure extremes (c.f., Fig. 5), and thus impulses applied to the power piston will be maximized and minimized in the appropriate directions. This intuitively shows how maximum power is transferred to the power piston. The two piston trajectories appear to be approximately 90 deg out of phase, though it is a little difficult to unambiguously measure phase shifts for nonsinusoidal signals. We note, however, that this phase shift is an outcome of the optimization rather than being enforced with kinematic linkages as is the case in traditional Stirling engines.

For comparison, the optimal displacer and power piston trajectories for the beta model are shown in Fig. 6. Note how these motions resemble those of a pure sinusoid; this is primarily a result of the rotational inertia of the flywheel causing it to spin at near constant speed.

Finally, the pressure/volume (PV) diagrams for both the beta and optimally actuated models are shown in Fig. 7. The areas enclosed by the two models are very similar in size, so they produce roughly the same energy per cycle. However, the operating frequency of the actuated model is faster than that of the beta model (as can be seen when comparing Figs. 5 and 6), so it completes more cycles in a given amount of time. The end result is that the optimally actuated model produces 42% more power than the optimally designed beta model.

A natural question is what the performance of the beta engine would be if operated at the faster frequency that is optimal for the actuated engine? However, in order to insure a valid comparison between the two engines, the only changes which can be made to the beta engine design are those used in the construction of the flywheel; thus, this is the only way the operating frequency can be adjusted. Since the flywheel parameters were already optimized for maximum average net power, any alteration to their values would result in decreased performance.

5 Conclusions

We have shown how the framework of OPC can be used to design optimal cycles for displacer-actuated Stirling engines. The performance objective is the net power harvested by the engine from the heat reservoirs' temperature difference. Both the optimal engine's cycling frequency as well as the optimal piston motion waveforms are obtained as a result of the optimization. The optimal waveforms show significant higher harmonic content, and displacer piston motions in particular are closer to square waves than they are to pure sinusoids. The operating frequencies are also different from those that result from optimized kinematic linkages. A case study was presented where an optimally actuated engine produced 42% more mechanical power than a comparable, best-case-design kinematically linked engine.

This work is a starting point for the use of OPC for actuated Stirling engine optimization. One of the major drawbacks of the isothermal Schmidt model is the assumption of instantaneous heat transfer from the external reservoirs to the working gas. Current work includes the application of the OPC framework presented here to higher fidelity models of the Stirling engine which incorporate finite-rate heat transfer, as well as more detailed models of regenerator dynamics. We expect that OPC would be even more critical and beneficial in these more complex models.

On a more general note, it is likely that OPC is the proper framework for a large class of energy conversion and harvesting problems. Cyclic operation is natural in such problems, and when active actuation is introduced, the role of OPC is to find more energetically favorable limit cycles than the ones that would occur naturally without active actuation. We have demonstrated this idea for a simple Stirling engine model in the present work, but we believe this basic framework to be applicable to several other energy conversion problems as well.

Acknowledgment

This work was partially supported by the NSF CMMI-1363386.

Appendix

Existence of Periodic Solutions to Periodically Time-Varying Systems

The equivalence of the first and second clause of Theorem 1 is a simple argument that was outlined in the text leading to Eq. (35). It remains to show the equivalence of the second and third clauses.

Considering the matrix–vector equation (37) and recall two fundamental facts from linear algebra. A matrix–vector equation of the form

$$M\bar{\lambda} = w$$

has a solution $\bar{\lambda}$ if and only if (iff) the vector w is in the range (column span) of the matrix M, i.e., $w \in \mathcal{R}(M)$. The second fact is that for any matrix, its range and the null space of its adjoint are orthogonal and complementary, i.e.,

$$\mathcal{R}(M) \perp \mathcal{N}(M^T)$$

This means that $w \in \mathcal{R}(M)$ iff it is perpendicular to every element of the null space of M^T, i.e.,

$$w \in \mathcal{R}(M) \;\Leftrightarrow\; \forall \bar{z} \text{s.t.} M^T\bar{z} = 0, \quad \bar{z}^T w = 0 \tag{A1}$$

Now applying this to the matrix–vector equation (37), we see that the condition $M^T\bar{z} = 0$ amounts to $\left(I - \Phi^T(T,0)\right)\bar{z} = 0$. The latter statement is equivalent to

$$\bar{z} = \Phi^T(T,0)\bar{z} \;\Leftrightarrow\; \Phi^T(0,T)\bar{z} = \bar{z}$$

since $\left(\Phi^T(T,0)\right)^{-1} = \Phi^T(0,T)$. It is well known that $\Phi_a(T,\ 0) = \Phi^T(0,\ T)$ is the state transition matrix of the adjoint system

$$\dot{z}(t) = -A^T(t)z(t) \tag{A2}$$

and therefore the statement $\Phi^T(0,T)\bar{z} = \bar{z}$ is equivalent to the existence of a T-periodic solution of the system (A2) with $z(0) = z(T) = \bar{z}$. Finally, we rewrite the dot product term $\bar{z}^T w$ in Eq. (A1) as applied to Eq. (37)

$$\bar{z}^T \int_0^T \Phi(T,t)B(t)dt = \int_0^T \left(\Phi^T(T,t)\bar{z}\right)^T B(t)dt$$

and observe that the function $\Phi^T(T,.)\bar{z} = \Phi_a(.,T)\bar{z}$ is simply the solution of Eq. (A2) with the final boundary condition $z(T) = \bar{z}$, therefore a T-periodic solution.

In summary, applying the fundamental linear algebra result (A1) to the system (37) gives the following: for all $\bar{z}$ such that $\Phi^T(0,T)\bar{z} = \bar{z}$ (i.e., for all periodic solutions $z(.)$ of Eq. (A2)), we must have:

$$\int_0^T z^T(t)B(t)dt = 0$$

which is the second clause of the theorem.

References

[1] Kongtragool, B., and Wongwises, S., 2003, "A Review of Solar-Powered Stirling Engines and Low Temperature Differential Stirling Engines," Renewable Sustainable Energy Rev., **7**(2), pp. 131–154.

[2] Riofrio, J. A., Al-Dakkan, K., Hofacker, M. E., and Barth, E. J., 2008, "Control-Based Design of Free-Piston Stirling Engines," American Control Conference, IEEE, pp. 1533–1538.
[3] Hofacker, M., Kong, J., and Barth, E. J., 2009, "A Lumped-Parameter Dynamic Model of a Thermal Regenerator for Free-Piston Stirling Engines," ASME Paper No. DSCC2009-2741, pp. 237–244.
[4] Hofacker, M. E., Tucker, J. M., and Barth, E. J., 2011, "Modeling and Validation of Free-Piston Stirling Engines Using Impedance Controlled Hardware-in-the-Loop," ASME Paper No. DSCC2011-6105, pp. 153–160.
[5] Mueller-Roemer, C., and Caines, P., 2013, "Isothermal Energy Function State. Space Model of a Stirling Engine," ASME J. Dyn. Syst., Meas., Control (Submitted).
[6] Gopal, V. K., Duke, R., and Clucas, D., 2009, "Active Stirling Engine," TENCON 2009-2009 IEEE Region 10 Conference, IEEE, pp. 1–6.
[7] Ulusoy, N., 1994, "Dynamic Analysis of Free Piston Stirling Engines," Ph.D. thesis, Case Western Reserve University, Cleveland, OH.
[8] Speyer, J., and Evans, R., 1984, "A Second Variational Theory for Optimal Periodic Processes," IEEE Trans. Autom. Control, **29**(2), pp. 138–148.
[9] Speyer, J. L., Dannemiller, D., and Walker, D., 1985, "Periodic Optical Cruise of an Atmospheric Vehicle," J. Guid. Control Dyn., **8**(1), pp. 31–38.
[10] Speyer, J. L., 1996, "Periodic Optimal Flight," J. Guid. Control Dyn., **19**(4), pp. 745–755.
[11] Gilbert, E. G., 1976, "Vehicle Cruise: Improved Fuel Economy by Periodic Control," Automatica, **12**(2), pp. 159–166.
[12] Gilbert, E. G., 1977, "Optimal Periodic Control: A General Theory of Necessary Conditions," SIAM J. Control Optim., **15**(5), pp. 717–746.
[13] Sage, A. P., 1968, "Optimum Systems Control," Technical Report DTIC Document.
[14] Bryson, A. E., and Ho, Y.-C., 1975, *Applied Optimal Control: Optimization, Estimation, and Control*, Taylor & Francis, Boca Raton, FL.
[15] Kirk, D. E., 2012, *Optimal Control Theory: An Introduction*, Dover Publications, Mineola, NY.
[16] Horn, F., and Lin, R., 1967, "Periodic Processes: A Variational Approach," Ind. Eng. Chem. Process Des. Dev., **6**(1), pp. 21–30.
[17] Kowler, D. E., and Kadlec, R. H., 1972, "The Optimal Control of a Periodic Adsorber: Part II. Theory," AIChE J., **18**(6), pp. 1212–1219.
[18] van Noorden, T., Verduyn Lunel, S., and Bliek, A., 2003, "Optimization of Cyclically Operated Reactors and Separators," Chem. Eng. Sci., **58**(18), pp. 4115–4127.
[19] Yakubovich, V., and Starzhinskii, V., 1972, *Lineinye differentsial'nye uravneniya s periodicheskimi koeffitsientami* (*Linear Differential Equations With Periodic Coefficients*), Wiley, New York.